Quaternary Science Reviews 170 (2017) 121–135

Contents lists available at ScienceDirect

Quaternary Science Reviews

journal homepage: www.elsevier.com/locate/quascirev

6-kyr record of flood frequency and intensity in the western Mediterranean Alps – Interplay of solar and temperature forcing☆

Sabatier Pierre [a, *], Wilhelm Bruno [b], Ficetola Gentile Francesco [c, d], Moiroux Fanny [a], Poulenard Jérôme [a], Develle Anne-Lise [a], Bichet Adeline [b], Chen Wentao [c, d], Pignol Cécile [a], Reyss Jean-Louis [a], Gielly Ludovic [c, d], Bajard Manon [a], Perrette Yves [a], Malet Emmanuel [a], Taberlet Pierre [c, d], Arnaud Fabien [a]

[a] EDYTEM, Université Savoie Mont Blanc, CNRS, 7337 Le Bourget du Lac, France
[b] LTHE, Université Grenoble Alpes, 38000 Grenoble, France
[c] Laboratoire d'Ecologie Alpine, Université Grenoble Alpes, F-38000 Grenoble, France
[d] Laboratoire d'Ecologie Alpine, CNRS, F-38000 Grenoble, France

ARTICLE INFO

Article history:
Received 15 December 2016
Received in revised form
9 June 2017
Accepted 22 June 2017

Keywords:
Holocene
Paleoclimatology
Western mediterranean alps
Sedimentology
Flood frequency and intensity
Lake sediment
Human activity
Ancient DNA
Earthquakes

ABSTRACT

The high-resolution sedimentological and geochemical analysis of a sediment sequence from Lake Savine (Western Mediterranean Alps, France) led to the identification of 220 event layers for the last 6000 years. 200 were triggered by flood events and 20 by underwater mass movements possibly related to earthquakes that occurred in 5 clusters of increase seismicity. Because human activity could influence the flood chronicle, the presence of pastures was reconstructed through ancient DNA, which suggested that the flood chronicle was mainly driven by hydroclimate variability. Weather reanalysis of historical floods allow to identify that mesoscale precipitation events called "East Return" events were the main triggers of floods recorded in Lake Savine. The first part of this palaeoflood record (6–4 kyr BP) was characterized by increases in flood frequency and intensity in phase with Northern Alpine palaeoflood records. By contrast, the second part of the record (i.e., since 4 kyr BP) was phased with Southern Alpine palaeoflood records. These results suggest a palaeohydrological transition at approximately 4 kyr BP, as has been previously described for the Mediterranean region. This may have resulted in a change of flood-prone hydro-meteorological processes, i.e., in the balance between occurrence and intensity of local convective climatic phenomena and their influence on Mediterranean mesoscale precipitation events in this part of the Alps. At a centennial timescale, increases in flood frequency and intensity corresponded to periods of solar minima, affecting climate through atmospheric changes in the Euro-Atlantic sector.

1. Introduction

Storms and floods are the most frequent and costly extreme weather events occurring in Europe and represented 69% of the economic losses caused by natural disasters between 1980 and 2006 (CEA, 2007). In mountain areas, river flooding is one of the most significant natural hazards, causing widespread damage to infrastructure as well as human and economic losses (Gaume et al., 2009). Therefore, robust knowledge about future trends of storms and floods is one of the main scientific challenges for a worldwide sustainable development. This is particularly true for the European Alps, with their recent demographic and touristic development (Beniston and Stephenson, 2004) and because of the high sensitivity of this region to ongoing climate warming. For the next century, a modification of the hydrological cycle is expected that may lead to changes in precipitation regimes and flood hazards. However, the projections of flood risk are still uncertain, mainly because of the complexity of precipitation pattern variations at a regional scale (IPCC, 2013). A recent study simulated a broad-scale reduction of summer precipitation in the Alps by the year 2100 but an increase in extreme precipitation events over high elevation areas associated with increased convective rainfall (Giorgi et al., 2016). A similar pattern was reported for the last two millennia

☆ The Lake Savine flood deposit data reported in this paper are deposited on NOAA Paleo: https://www.ncdc.noaa.gov/paleo/study/22278.

* Corresponding author.
E-mail address: pierre.sabatier@univ-savoie.fr (S. Pierre).

http://dx.doi.org/10.1016/j.quascirev.2017.06.019
0277-3791/

from the geological flood records of the Northern French Alps in which warmer periods correspond to a lower frequency but higher intensity of extreme flood events (Giguet-Covex et al., 2012; Wilhelm et al., 2013). However, the spatial and temporal distribution of flood events may be rather heterogeneous in the European Alps (Beniston et al., 2007; Giorgi et al., 2016). Additionally, the lack of long-term instrument data at high-elevation sites precludes the identification of significant trends (Beniston et al., 2007; Westra et al., 2013). Therefore, effects of modern climate change on the frequency and the intensity of extreme precipitation events are regionally difficult to anticipate. To overcome this issue, geological data offer opportunities to reconstruct long-term chronicles of past flood events well beyond observational records. Among the geological data, lake sediments are particularly suitable because they provide a well-preserved continuous archive of past flood events (Noren et al., 2002; Bøe et al., 2006; Moreno et al., 2008; Wilhelm et al., 2012a, 2013; Vannière et al., 2013; Wirth et al., 2013; Glur et al., 2013; Swierczynski et al., 2013; Corella et al., 2014; Czymzik et al., 2016).

This study focused on the reconstruction of past flood variability in a French-Italian Alpine border region mainly influenced by the Mediterranean climate. Over instrumental period, heavy precipitation events that triggered catastrophic floods were related to either local convective phenomena (i.e., summer thunderstorms) or mesoscale convective systems called “East Return” events strongly linked to the cyclonic activity across the Mediterranean area (Garavaglia et al., 2010; Gottardi et al., 2010). The main objective of this study was to identify regional flood patterns using historical and lacustrine (Lake Savine) archives. We present a well-dates and high-resolution multi-proxy study of a lake sediment core associating sedimentological and geochemistry data. Our approach focused on six challenges: (i) identify event layers at the millimetre scale, (ii) distinguish event layers induced by floods from those induced by mass movements, (iii) reconstruct the intensity of past floods, (iv) assess the potential impact of human activities on the recorded flood signal through ancient DNA, (v) define the type of precipitation events triggering floods by the study of weather reanalysis and (vi) discuss the long term variability of palaeoflood frequency and intensity with regard to past climatic variations.

2. Study area

2.1. Lake Savine and its catchment area

Lake Savine is located in the western Mediterranean Alps at the French-Italian border in the Haute-Maurienne massif (Fig. 1), approximately 90 km south of Lake Anterne (Giguet-Covex et al., 2011 Figs. 1b) and 105 km north of Lake Allos (Wilhelm et al., 2012a, Fig. 1b). The lake is a rectangular-shaped (550 × 175 m) high-elevation system (2447 m a.s.l., N45°10.500, E6°54.821). Its watershed is formed by a cirque of 3.5 km^2 limited in the southeastern part by the French-Italian border and rises to 3310 m a.s.l. It is mainly (90%) composed of crystalline rocks, Permian gneiss and mica schist. The upper northeastern part of the watershed is composed of Mesozoic rock with Triassic quartzite, dedolomitised breccia (locally named cargneule) and evaporites as well as of Jurrassic to Cretaceous marble and calcareous schist (Fig. 1c).

The main stream of the watershed (Torrent de Savine) drains the southeastern part and has built an alluvial plain (Fig. 1c) that suggests high detrital fluxes. The only evidence of past glacial activity is a moraine in the upper southwestern part of the watershed. Detrital inputs from this stream are limited to summer and autumn because the catchment is covered by snow and the lake is frozen from mid-November to mid-June. The Torrent de Savine flows downstream into the Ambin torrent and then joins the Arc river at the village of Bramans 12 km northwest of Lake Savine. The lake is located above the tree line.

2.2. Hydro-climatic setting and historical flood record

The climate of the study area is influenced by the Mediterranean Sea (Durant et al., 2009). Consequently, the Haute-Maurienne massif corresponds to a transition zone of Alpine precipitation patterns in meteorological reanalyse data between the Southern and the central French Alps (Durant et al., 2009). Heavy precipitation events are related to either local convective phenomena (i.e., summer thunderstorms) or mesoscale convective systems called “East Return” events that mainly occur from late spring to autumn, resulting from Mediterranean humid air masses flowing northward into the Po plain and then westward to the Haute-Maurienne Massif (Gottardi et al., 2010; Wilhelm et al., 2016a). Local historical documents (ONF-RTM database, http://rtm-onf.ifn.fr/) have provided evidence of numerous past flood events. This historical information shows that the village of Bramans has been affected by floods of the Ambin torrent and its two main tributaries (Savine and Etache torrents) at least 15 times during the last 150. Those of June 1957 and October 2000, were extreme precipitation events that resulted in significant damage to houses and infrastructure and cause several deaths (Ratto et al., 2003; Arnaud-Fassetta and Fort, 2004).

3. Material and methods

3.1. Lake coring

A 775-cm-long sediment core was extracted in March 2014 from the frozen surface of Lake Savine using an Uwitec piston coring device directly from the ice-covered surface of the lake. The core was retrieved from the deepest part of the lake (7-m depth, N45°10.500, E6°54.821). The sediment sequence SAV14 (IGSN codes refer to an open international database, www.geosamples.org) was composed of two overlapping coring holes, SAV14-01 and SAV14-02, made of three and two sections, respectively. Sections from the second hole were taken following a 1-m shift in depth to ensure a sufficient overlap to provide a continuous record. A short gravity core (SAV14P2) was also taken to provide a well-preserved water–sediment interface that was subsequently correlated to the composite sequence. The cores were split into two halves at the EDYTEM laboratory. Each half-section was described in detail and pictures were taken at a 20-pixel mm^{-1} resolution. Lithological description of the sequence allowed the identification of different sedimentary facies. A composite sediment sequence named SAV14 was built using distinct marker layers from the overlapping sections of parallel holes (SI1).

3.2. Sedimentary analysis and geochemistry

The grain-size distribution on most of the identified event layers was measured with a 5-mm sampling step using a Malvern Mastersizer 2000G laser particle sizer. Ultrasounic was used to dissociate mineral particles and to avoid flocculation. We then used the median (D50) and the coarsest (D90) fractions to characterize interbedded deposits (Passega, 1964; Mulder et al., 2001; Wilhelm et al., 2013, 2015). We also recorded the thickness and D90 max (i.e., the highest D90 value) of each interbedded deposit.

78 samples of 2-cm wide were sampled on specific interval along the SAV14 mastercore. After taking the inner part for ancient DNA analysis, external parts were dried at 60 °C over 4 days to obtain dry bulk densities. Then, the Loss Of Ignition (LOI) of each sample was determined using the protocol of Heiri et al. (2001). The

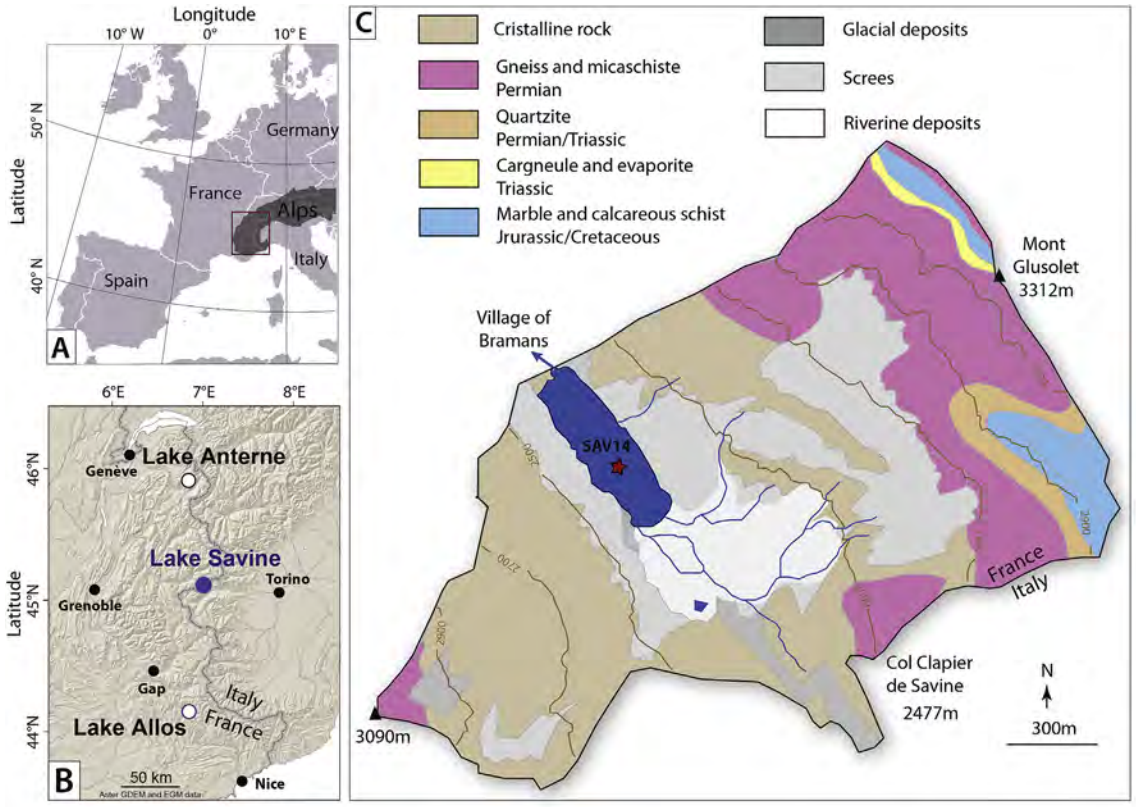

Fig. 1. (A) Location of Lake Savine in the Western Mediterranean Alps, (B) compared with the locations of Lake Anterne (Giguet-Covex et al., 2011) and Lake Allos (Wilhelm et al., 2012a). (C) Geological and geomorphological characteristics of the Lake Savine catchment area.

LOI at 550 °C and 950 °C corresponds to the organic and carbonate components of the sediment, respectively.

X-Ray Fluorescence (XRF) analysis was performed for the entire composite sequence with a 1-mm sampling step using the non-destructive Avaatech core-scanner (EDYTEM). The split core surface was first covered with 4-μm-thick Ultralene foil to avoid contamination of the XRF measurement unit and desiccation of the sediment. The geochemical data were obtained with two tube settings: 10 kV and 1.5 mA for 20 s for Al, Si, S, K, Ca, Ti, Mn, and Fe and 30 kV and 0.8 mA for 40 s for Cu, Zn, Br, Sr, Rb, Zr, and Pb (Richter et al., 2006). Each individual power spectrum was converted by a deconvolution process into relative components (intensities) expressed in counts per second.

3.3. Ancient DNA (aDNA)

The 78 slices of 2-cm thickness were sampled following the strict laboratory precautions described in Giguet-Covex et al. (2014). For each sediment slice, we mixed 15 g of sediment with 15 ml of saturated phosphate buffer (Na2HPO4; 0.12 M; pH ≈ 8) for 15 min. The mixture was then centrifuged (10 min at 10,000 × g), and 12 ml of the resulting supernatant were transferred to Amicon® Ultra-15 10 K Centrifugal Filter Devices (Millipore) and centrifuged (20 min at 4000 × g) for concentration of aDNA. Of the resulting concentrate, 400 μl was kept as starting material for DNA extraction, using the NucleoSpin® Soil kit (Macherey-Nagel) (Taberlet et al., 2012). Four extraction controls were performed. Mammal DNA was amplified with the primer pair Mam-P007 following the protocol described in Giguet-Covex et al. (2014). In addition to extraction controls, we performed three PCR control runs containing PCR mix but no DNA template and four PCR positive controls, each containing 0.18 ng of DNA extracted from a marsupial (*Dideplhis marsupialis*) absent in Europe. All samples and controls were amplified in 12 replicated PCRs (Ficetola et al., 2015). Sequencing was performed by 2 × 125 bp paired-end sequencing on the Illumina HiSeq 2500 platform, which returned 21,192,000 reads.

DNA sequences were filtered using the OBITOOLS software (Boyer et al., 2016) as described in Pansu et al. (2015). Sequences were assigned to the relevant taxa by comparing them with a global mammal database generated from EMBL using the *ecotag* programme. We only kept sequences with a match >97% with a mammal genus. In aDNA studies, false detections (i.e., sporadic detections of absent species) are possible. Therefore, we only considered species confirmed by multiple PCR analyses performed on the same sample, and we discarded sequences detected with <5 reads in each PCR replicate and sequences frequently detected in controls (humans and pig). We used site occupancy-detection modelling to estimate the detection probability of species and the frequency of false detections (Ficetola et al., 2015). Occupancy modelling was performed using Bayesian models, following Lahoz-Monfort et al. (2016). Estimates of occupancy, detection probability and the probability of false detection were then used to calculate the probability of species presence in each sample. This approach allowed the successful limiting of false positives in aDNA analyses, and the probability of presence was a measure of the reliability of species presence in a sample (Ficetola et al., 2016; Lahoz-Monfort et al., 2016).

3.4. Chronology

The chronology of the Lake Savine sediment sequence was

based on short-lived radionuclide measurements and 12 ^{14}C measurements on terrestrial macro-remains. The short-lived radionuclides in the upper 12 cm of core SAV14P2 were measured using high-efficiency, very low-background, well-type Ge detectors at the Modane Underground Laboratory (LSM) (Reyss et al., 1995). The measurement intervals followed facies boundaries and resulted in a non-regular sampling of approximately 5 mm. The isotope ^{137}Cs was accidentally introduced into the environment at the end of the 1950s as by-product of atmospheric nuclear weapons tests (peak at AD 1963). The Chernobyl accident in 1986 also dispersed ^{137}Cs into the northern atmosphere (Appleby, 1991). ^{210}Pb excess was calculated as the difference between total ^{210}Pb and ^{226}Ra activities (Golberg, 1963). We then used the Constant Flux/Constant Sedimentation (CFCS) model and the decrease in excess ^{210}Pb to calculate sedimentation rates (Golberg, 1963). The uncertainty of sedimentation rates obtained by this method was derived from the standard error of the linear regression of the CFCS model. The ^{14}C measurements were carried out by an Accelerator Mass Spectrometer (AMS) at the Laboratoire de Mesure ^{14}C (LMC14) ARTEMIS at the CEA (Atomic Energy Commission) institute at Saclay (Table 1). The IntCal13 calibration curve (Reimer et al., 2013) was used for ^{14}C age calibration. Then, we used the software-package "clam" (version 3.0.2 R Development Core Team, 2011) to generate an age/depth model (Blaauw, 2010).

3.5. Weather analysis

Weather analyses were realized using the 20th-century reanalysis (version 2) product of Compo et al. (2011), which contains global atmospheric variables since 1871 on a 2° grid (hereafter 20CR). The reanalysis is based on the Ensemble Kalman Filter data assimilation system of Whitaker and Hamill (2002) and assimilates observed surface pressure and sea-level pressure every 6 h. All reanalysis data used in the current study were related to the mean of the 56 ensemble members. The atmospheric circulation patterns associated with historical flood events recorded in Lake Savine were based on a daily mean of 500 hPa geopotential height anomalies (Z500) and vertically integrated water vapor transport (hereafter IWT). IWT was computed from the daily fields of specific humidity (q), zonal (u), meridional (v) winds and differential of pressure (dp). The magnitude of daily IWT was calculated in an Eulerian framework as follows:

$$IWT = \left[\left(\int_{1000}^{300} qu \frac{dp}{g} \right)^2 + \left(\int_{1000}^{300} qv \frac{dp}{g} \right)^2 \right]^{\frac{1}{2}}$$

where g is the acceleration due to gravity. The vertical integration was limited to the 1000 to 300 hPa pressure interval because specific humidity in the 20CR data is negligible above 300 hPa. Through the manuscript D represents the day of historical precipitation event, D-2, D-1 mean two and one days before D respectively.

4. Results

4.1. Core description and lithology

The upper 7 m of sediment consisted of dark to very dark olive silt composed of 5 ± 1.3% of LOI550 (organic matter, OM) and 7.5 ± 1% of LOI950 (Carbonate fraction) representing the background hemi-pelagic sedimentation (named BS for background sedimentation, Fig. 2). Below 7 m the sediment consisted of homogenous light grey clay to silt with 2 ± 0.1% LOI550 and 6.8 ± 0.1% of LOI950. Because no plant macro-remains requested for (radiocarbon) dating were found deeper than 5.7 m, this study is focused on the upper 5.7 m of the Savine sedimentary record. These fine grained deposits were interrupted by 220 graded layers that are interpreted to represent short-term depositional events according to Sturm and Matter (1978) and Arnaud et al. (2002).

The 220 event layers were divided in two types of deposits based on their grain size and geochemical patterns. Type-1 (T1) deposits were light-grey graded bed with no evidence of an erosive base (Fig. 2). The 200 T1 deposits are characterized by a silty-to-sandy base, a central part with a regular decrease of both D50 and D90 and a very light-grey clayey cap (Fig. 2). The bottom of T1

Table 1
^{14}C dates for Lake Savine. Samples in bold correspond to rejected dates.

Samples	Material dated	Cores	Composite depth (mm)	Depth without instantaneous deposits (mm)	Uncalibrated age (BP)	Uncertainty	Calibrated age ranges at 95% confidence interval (cal. BP)
SacA38347	**Organic macroremain**	**SAV02A**	**355**	**225**	**450**	**30**	**473–535**
SacA38348	Organic macroremain	SAV02A	655	275	405	30	329–516
SacA38349	**Organic macroremain**	**SAV02A**	**885**	**350**	**895**	**30**	**737–909**
SacA38350	Organic macroremain	SAV02A	1265	455	645	30	556–668
SacA38351	Organic macroremain	SAV01A2	1520	535	1100	30	938–1062
SacA38352	Organic macroremain	SAV01A2	1775	560	1315	30	1179–1296
SacA38353	Organic macroremain	SAV01A2	2310	679	1740	30	1564–1714
SacA39966	Organic macroremain	SAV01A2	2765	851	1985	30	1878–1994
SacA38354	Organic macroremain	SAV02B1	3465	1036	2525	40	2472–2745
SacA38355	Organic macroremain	SAV01B2	4425	1397	3560	30	3725–3963
SacA38356	Organic macroremain	SAV01B2	5265	1633	4485	35	4980–5294
SacA38357	Organic macroremain	SAV02C1	5655	1866	5260	35	5932–6178

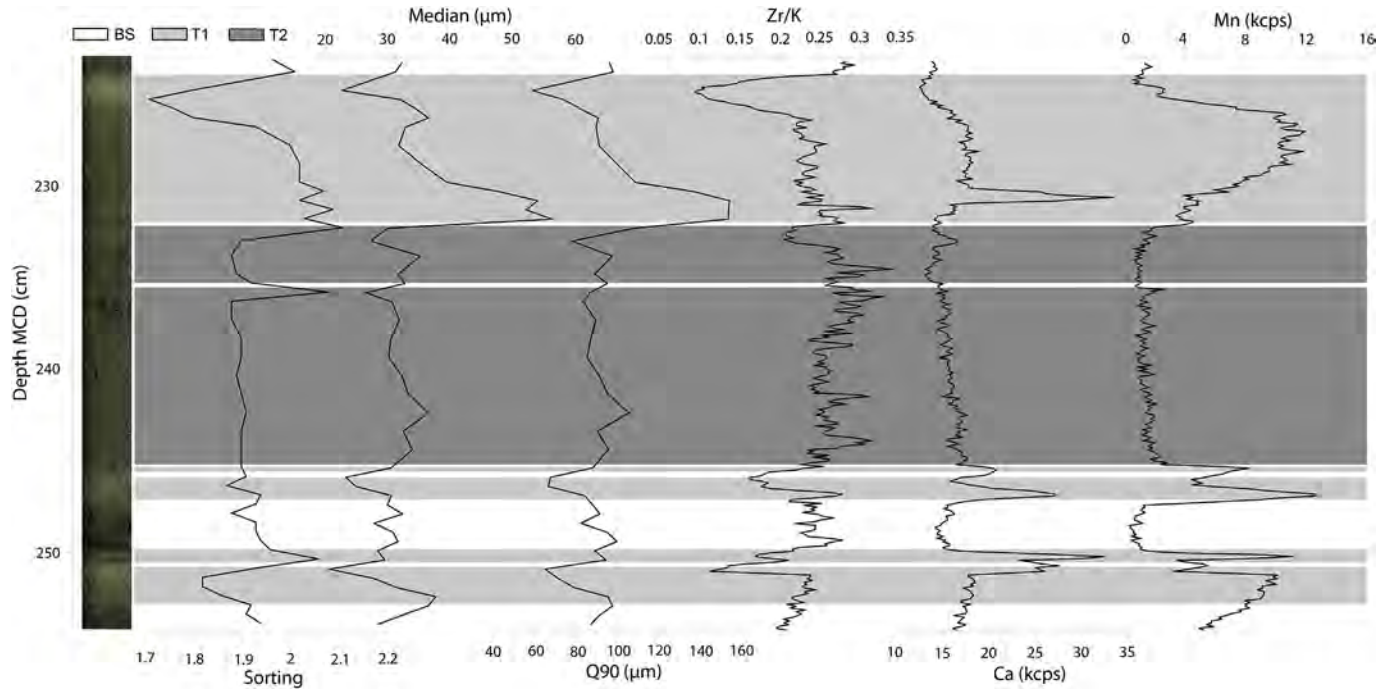

Fig. 2. Photography, grain size and geochemical data examples of the three sedimentary facies of SAV14 (BS: background sedimentation in white, T1 in light grey and T2 dark grey).

deposits are characterized by relatively high sorting values (mostly > 2, Fig. 2). Their geochemical pattern is characterized by relatively high Zr intensities at the base and high K intensities in the clay cap, suggesting Zr enrichment in the coarser sediment fraction and K enrichment in the finest fraction. The Zr/K ratio was thus supposed to be a high-resolution proxy of grain-size (Wilhelm et al., 2013; Arnaud et al., 2016). However, the relation between the Zr/K ratio and grain size parameters is not well constrained, probably in relation to different sample resolutions (1 mm and 5 mm respectively). Thus this geochemical ratio thus cannot be used as a high-resolution grain-size proxy but was used to identify T1 deposits. Ca intensities in these deposits showed high values (Fig. 2) simultaneous with high values of LOI950, which suggests high carbonate contents. This increase in Ca reflects detrital calcareous input from the eastern part of the watershed related to torrential activity (thanks to detailed Scanning Electron Microscopy (SEM) analysis, data not shown). Mn intensities also showed high values in T1 deposits (Fig. 2) that probably reflect the oxygenation state of the water column (Calvert and Pedersen, 1993; Elbaz-Poulichet et al., 2014). The thickness of T1 deposits varied between 2 and 170 mm with a mean of 20 mm (Fig. 3).

Type-2 (T2, Fig. 2) deposits were composed of homogeneous, olive to grey, basal silty layers topped by light grey mm-thick clay caps. Their grain size parameters (median, D90) did not show any significant variations except for the clay cap, where lower values of median and D90 were observed (Fig. 2). The sorting of T2 deposits always presented weak values (approximately 1.9) except for the uppermost samples of each deposit because the clay cap is very thin and thus a mix with the silts of the background sediment. Geochemical data presented a constant and relatively high Zr/K ratio, except for the clay cap, and low values of Ca and Mn intensities (Fig. 2).

Plotting the thickness of all T1 (n = 26) and T2 (n = 16) deposits thicker than 1 cm versus D90 max (Wilhelm et al., 2012a,b) highlights two distinct patterns (Fig. 3). A significant positive linear relationship between bed thickness and D90 max (r = 0.94, $p < 10^{-12}$) was observed for T1 deposits (Fig. 3). This suggests that the grain size of the mobilized sediments is larger when the volume of sediments transported and deposited is higher. For the T2 deposits, a distinct pattern was observed of a high variability of deposit thickness without high variations in D90 max. This suggests that the volumes of sediments transported and deposited to form T2 deposits were poorly related to grain size and thus to underwater current velocities.

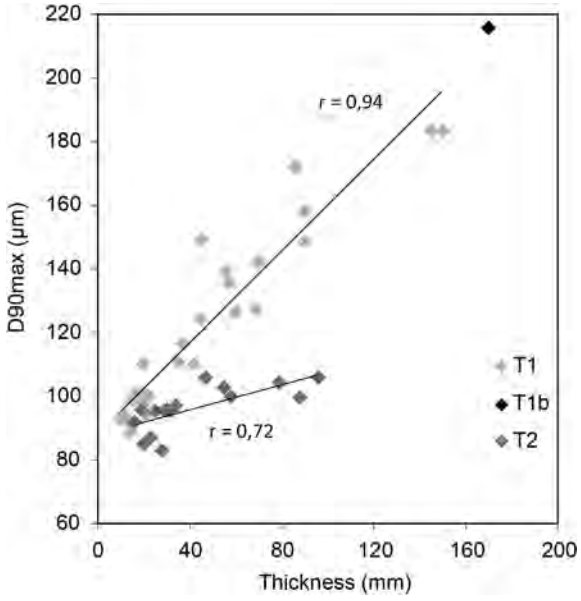

Fig. 3. Diagram of the D90 max-deposit thickness for T1 and T2 deposits. T1b corresponds to the mass movement-induced deposit above the reversed sequence; see SI3.

Finally, a remarkable 22-cm thick reversed sequence was observed between 196 and 218 cm depth of the master core overlapped by a 17-cm thick graded layer (detailed in SI3). This T1

deposit, labelled as T1b in Fig. 3, corresponds to the thickest layer of the entire sequence and was not considered in the comparison of grain size thicknesses. It was localized at the top of the reversal sequence (SI3) and have the same characteristic than other T1 deposits.

4.2. Chronology

4.2.1. Short-lived radionuclides

The excess ^{210}Pb downcore profile showed a regular decrease punctuated by distinct drops (Fig. 4). Following Arnaud et al. (2002), these low values of ^{210}Pbex corresponded to T1 deposits and were excluded from the construction of an event-free sedimentary record because they were considered as instantaneous deposits. ^{210}Pbex activities plotted on a logarithmic scale revealed two linear trends providing two mean sedimentation rates of 1.39 ± 0.2 mm yr^{-1} above 4.5 cm and 0.44 ± 0.04 mm yr^{-1} below. Ages were then calculated using the CFCS model applied to the original sediment sequence to provide a continuous age-depth relationship.

The ^{137}Cs profile presented one peak at 4.5 cm with a high activity of 692 ± 6 Bq.kg^{-1}. This corresponds to the Chernobyl accident in 1986 CE, and the localization of the study site at the border between France and Italy strengthened this interpretation because Italy had larger ^{137}Cs fallout from this accident. The ^{137}Cs activity from maximum nuclear weapon tests in the Northern Hemisphere in 1963 CE presents a regional value between 40 and 300 Bq. kg^{-1} (Wilhelm et al., 2012b; Jenny et al., 2013; Alric et al., 2013; Sabatier et al., 2014; Bajard et al., 2015; Guédron et al., 2016). Such a ^{137}Cs activity was reached at approximately 5.8 cm, even if this ^{137}Cs peak is not clearly identifiable probably in relation to the sample resolution. Both artificial markers are in agreement with the CFCS age model for the last century (Fig. 4).

4.2.2. Radiocarbon dating

A total of 12 terrestrial organic macroremain samples were dated by ^{14}C age (Table 1). Two radiocarbon ages were excluded because they appear to be too old, probably due to macroremain stored in the lake catchment and would result in age inversions (Fig. 5). The 220 deposits interpreted as instantaneous events and the reversed sequence (SI3, noted R in Fig. 5), representing a total of 391 cm were removed. The remaining 200 cm (Fig. 5A) were used to build an event-free sedimentary record (Bøe et al., 2006; Wilhelm et al., 2012a, 2013, Fig. 5A). We then calculated an age-depth relationship by a smooth spline interpolation using the R-code package "Clam" version 2.2 (Blaauw, 2010). This age-depth

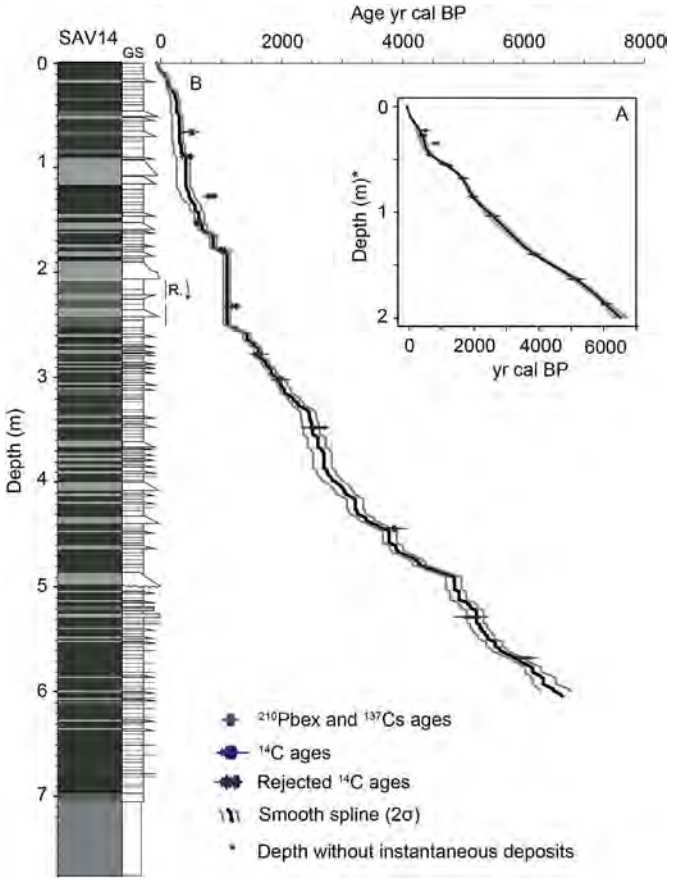

Fig. 5. (A) Age-depth model of the event-free sediment record based on radiocarbon- and short-lived radionuclides-derived ages. (B) Age-depth model for the entire SAV14 sediment sequence. Colour is defined is SI2. R indicates the reversed sequence; see SI3. GS: grain size. (For interpretation of the references to colour in this figure legend, the reader is referred to the web version of this article.)

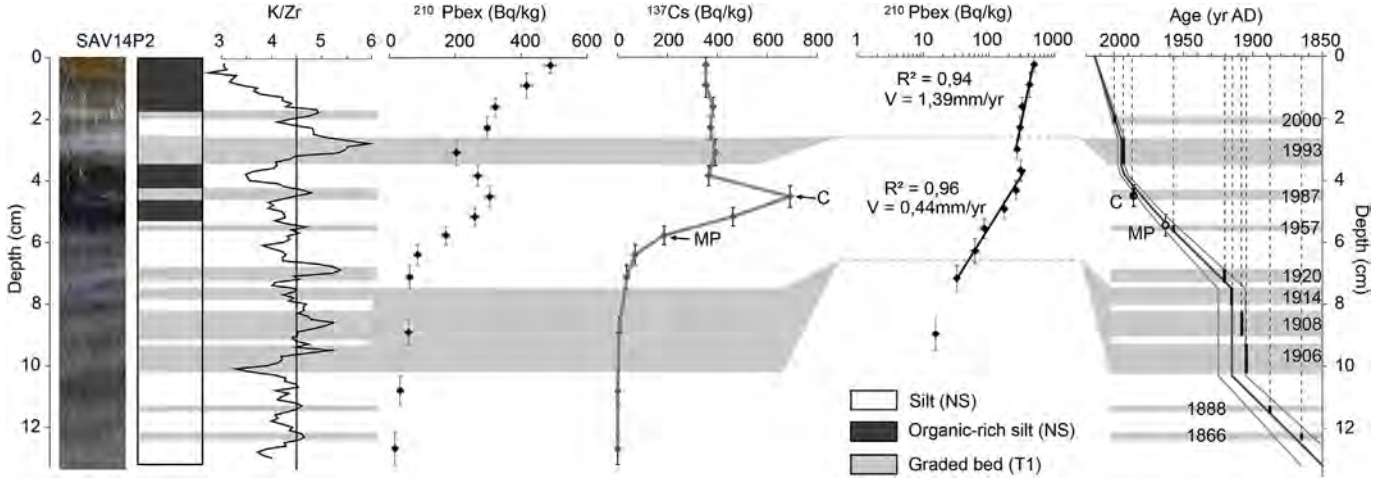

Fig. 4. Chronology (with 1σ uncertainties) of the uppermost part of core SAV14P2 based on short-lived radionuclides (^{210}Pbex and ^{137}Cs) and application of the CFCS model to the event-free ^{210}Pbex profile. Uncertainties of ^{210}Pbex and ^{137}Cs activities are included in dots. Dates on the right-hand side correspond to dates of historical floods, possibly associated with the most recent T1 deposits.

model was used to date all instantaneous deposits. The vertical bars represent the age of each flood thicker than 5 mm with uncertainties (2σ) resulting from the ^{14}C ages (Fig. 5B). The first 565 cm of the sediment sequence from Lake Savine covered the last 5.8 kyr BP. The mean sedimentation rates estimated from the event-free sediment record varied between 0.2 and 0.4 mm yr^{-1} with a short-term increase to 0.6 mm yr^{-1} between 1.95 and 1.65 kyr BP, to 1.4 between 0.35 and 0.55 kyr BP and to 0.44 during the last 40 years (Fig. 6D).

4.3. Ancient DNA

We detected DNA of the taxa of four mammals: *Bos* (cattle), *Canis* (dog), *Felis* (cat) and *Ovis* (sheep). However, only cattle and sheep DNA was detected in more than one sample by multiple PCR replicates. Therefore, we focused the analyses on these two species, whereas we assumed the presence of dog and cat DNA to be sporadic.

But also cattle DNA occurred sporadically in sediments older than 2460 yr cal BP (below 332 cm depth). However, in these cases, sheep DNA was only detected in one of the 12 PCR replicates performed on each sediment slice. Consequently, the reliability of sheep detections was low. Conversely, cattle and sheep DNA was consistently detected between 2050 and 1750 yr cal BP (289 and 307 cm) in multiple PCR replicates per sample, which indicates high reliability of their presence in this short period (Fig. 6E and F) (Giguet-Covex et al., 2014).

5. Discussion

5.1. Event layers

5.1.1. Flood-induced layers

Normally graded layers like T1 deposits are common features of lake sediments, where they are associated with turbidity currents triggered by mass movements or flood events (Sturm and Matter, 1978; Arnaud et al., 2002; Gilbert et al., 2006). In the thickness–D90 max diagram, T1 deposits are grouped in a distinct cluster, which suggests that they resulted from the same trigger mechanisms (Fig. 3). Additionally, the increase of transported and deposited sediment volumes with grain size characterize T1 deposits (Fig. 3) as consistent with sedimentary processes regulated by flowing water currents (e.g., Wilhelm et al., 2013, 2015). Higher discharge rates lead to a larger sediment supply and coarser grains transported to the lake. The 200 T1 deposits are also characterized by increases in Mn, which suggests that changes in redox conditions occurred in the lake system. In oxic waters, Mn occurs as Mn(IV) and diffuses downwards where it can precipitate as MnCO3 or Mn–Ca carbonates (Calvert and Pedersen, 1993; Pedersen and Price, 1982) and upwards where it can precipitate as Mn oxides at the oxic/anoxic transition (Elbaz-Poulichet et al., 2014). This process leads to Mn enrichment at the oxygen-rich water-sediment interface (Calvert and Pedersen, 1993). When bottom waters are anoxic, Mn(II) diffuses to the water column and Mn becomes depleted in the sediments. The presence of Mn in the graded layers associated with Ca (Fig. 2) suggests that hyperpycnal turbidity currents favoured bottom water re-oxygenation (Wilhelm et al., 2016a) and produced rapid precipitation of Mn oxides and/or Mn–Ca carbonates in the sediment (Calvert and Pedersen, 1993).

To verify this hypothesis, we compared our record with the historical flood calendar from the Ambin torrent and its two main tributaries to the event layers archived in the lake sediment for the last 150 years. Ten historical flood events occurred in 2000 CE, 1993, 1987, 1957, 1920, 1914, 1908, 1906, 1888 and 1866 and correspond well to the age of T1 deposits identified by the Zr/K ratio of the uppermost 13 cm (Fig. 4). All these arguments support that T1 deposits were induced by floods.

To reconstruct the intensity of past floods, two proxies could be used; grain size and thickness of the flood deposits. The grain-size data are interpreted to represent the river energy and, thereby, the discharge (e.g. Campbell, 1998; Parris et al., 2010; Lapointe et al., 2012; Wilhelm et al., 2015). The grain-size distribution reflects hydrologic conditions, in particular transport capacity during a flood event, thus the maximum grain size (Q90 max) is a proxy of stream velocity during flood events (Molinaroli et al., 2009; Parris et al., 2010) and it could be applied to assess the intensity of past floods (Gilli et al., 2013). The thickness is interpreted to represent the total volume of solid transported material and deposited during the flood event (Schiefer et al., 2011; Wilhelm et al., 2012a, 2015; Jenny et al., 2014). The significant relationship between D90 max and thickness of T1 flood deposits (Fig. 3) suggests that both parameters could be used, but thickness is more easy measured on each flood layer this is why we choose thickness as a proxy of flood intensity.

5.1.2. Mass movement-induced layers

The thickness-D90 max diagram reveals that T2 deposits resulted from processes distinctly differs from those of T1 deposits. This diagram also suggests that the volume of transported and deposited sediments can vary largely without significant variations in grain size. The constant mean grain-size and the stable values of sorting are typical of mass-flow deposits (Mulder and Cochonat, 1996). T2 deposits showed only a thin fining-upward sequence followed by a thick homogenous interval with no inverse grading at the base. Additionally, these homogeneous layers did not present any increase of the Mn content (Fig. 2). This suggests that the turbidity currents that triggered T2 deposits did not allow oxygen to be carried to the deepest part of the basin and were thus probably related to subaquatic mass movements that reworked the sediment of the lake shores (Wilhelm et al., 2016b). A similar type of mass movement-induced facies in lacustrine environments has been previously described and called “homogenites” or “seiche deposits” (Chapron et al., 1999; Beck, 2009; Petersen et al., 2014). According to these authors, a large mass movement would induce an oscillatory movement of the whole lake-water mass. The related hyperpycnal (turbidity) currents would transport both the bed-load and suspended-load to the deepest part of the lake (Beck, 2009). The bed-load sediment would produce the coarse base of the layers, whereas the suspended-load sediment would be homogenized by the oscillation of the lake waters. Also, the remarkable reversed sequence topped by the T1b deposit (SI3) is probably related to a large subaquatic landslide due a mass movement or a very large flood, but this particular deposit is not take into account in the next sections.

5.2. Earthquake record

Earthquake shaking appears to be the most common factors that trigger mass movements in high-elevation alpine lakes (Wilhelm et al., 2016b). To test this observation, ages of most recent T2 deposits were compared with dates of regional historical earthquakes that are well documented over the last centuries (Lambert and Levret-Albaret, 1996; Scotti et al., 2004).

For this period, one T2 deposit was recorded in 1755 CE (between 1820-1710 CE at 2σ of uncertainty). To determine the earthquake that most probably triggered this deposit we follow the method provided by Wilhelm et al. (2016a,b), the epicentral MSK (Medvedev-Sponheuer-Karnik intensities) intensities of all historical earthquakes were plotted against the distance of each earthquake from the lake (Fig. SI4). The potentially recorded earthquakes

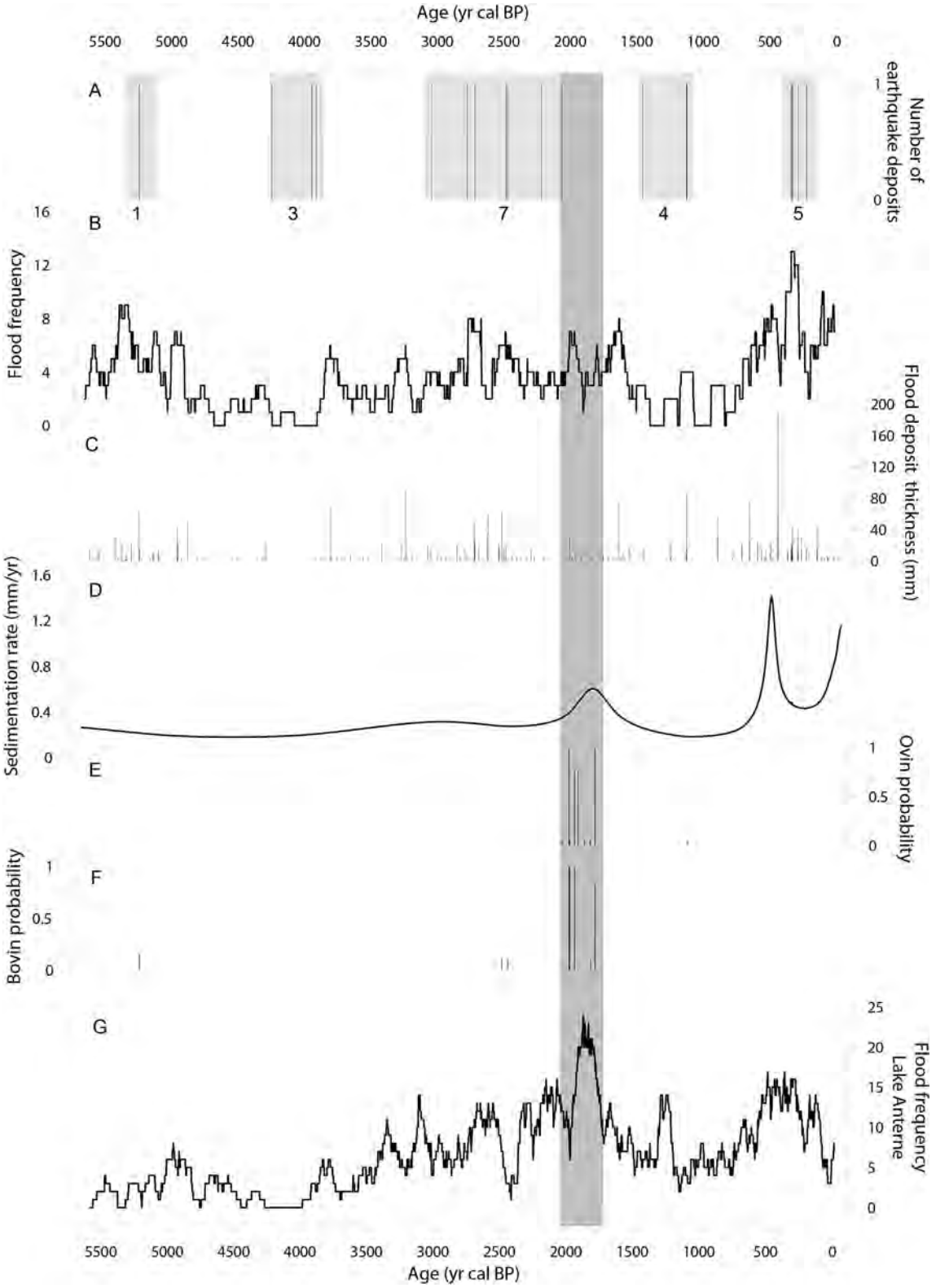

Fig. 6. Comparison of (A) reconstructed earthquake events (light grey bands represent periods of high seismic activity with the associated numbers of earthquakes during these periods), (B) flood frequency (101-yr running average) and (C) flood intensity (thickness of flood deposits), (D) average sedimentation rate without instantaneous deposits (earthquake and flood > 5 mm), (E) ovine and (F) bovine presence probability on the watershed. (G) Flood frequency of the Lake Anterne (101-yr running average) from Giguet-Covex et al. (2011); the vertical grey band is the period of high human activity in both the Savine and Anterne lake records.

are also expected to be the strongest and/or the closest to the lake, as those are expected to have generated the largest ground motions in the lake area. To take into account this second parameter, the seismic intensity of each historical earthquake in the lake area was estimated in first order by using the equation define by Wilhelm et al. (2016a,b) for this region. From this estimation, three earthquakes over the last 300 years triggered local seismic intensities above VI at 10 km from the catchment area of the Lake Savine, i.e. intensities that may be strong enough to trigger seismically induced deposits (Fig. SI4); in 1808 CE (Valle del Pellice, 8 MSK), 1785 CE (Valle del Susa, 7.5 MSK) and 1767 CE (Valle di Lanzo, 8 MSK) (Boschi et al., 2000). From this three earthquakes, the most recent and "strongest" historical earthquake occurring in 1785 CE, and could correspond to the most recent T2 deposit; dated at 1755 CE from our chronology (Fig. SI4).

A total of 20 T2 deposits supposedly induced by past earthquakes were identified. These deposits were spread in 5 clusters over the last 5.6 kyr cal BP covered by the sedimentary record (Fig. 6A). This suggests 5 periods of increased seismicity at approximately 5.22, 4.25–3.8, 3.1–2, 1.45–1.05 and 0.35–0.15 kyr cal BP. Interestingly, 10 out of 20 T2 layers presented no background sediment between adjacent deposits that can be interpreted as the record of earthquakes and respective aftershocks. The earthquake-induced deposit recorded at approximately 5.22 kyr cal BP (5.06–5.335 kyr at 2σ) can correspond to an event which was recorded at a regional scale in three other lakes located more than 115 km away in the Northern French Alps (lakes Le Bourget, Paladru and Blanc Huez; Chapron et al., 2016). This suggests the occurrence of a high magnitude earthquake.

The Earthquake Sensitivity Threshold Index, ESTI, defined by Wilhelm et al. (2016b), was estimated to be 0.15 ± 0.01 for Lake Savine, which is in the observed trend for other Alpine lakes. Note that the ESTI value was found to be highly dependent on the sedimentation rate (Wilhelm et al., 2016b). Because of high variations in sedimentation rate at Lake Savine (Fig. 5), its sensitivity to record earthquakes may have changed over time. However, despite the last cluster, these periods of relatively high earthquake occurrences mainly correspond to low sedimentation rates and could thus be associated with a regional cluster of seismicity, as it was observed for west Algeria by Ratzov et al. (2015).

5.3. Modification of erosion processes

The climatic information from the Savine flood record can be considered relevant for the last 5.6 kyr cal BP (Fig. 6B and C) if no major changes occurred in erosion processes. Erosion in the Savine catchment may be affected by geomorphological modifications and/or by land-use changes linked to human activities (i.e., grazing).

5.3.1. Geomorphological activity

Even if the modern watershed is not glaciated, substantial activity of small glaciers could have modified the sediment availability during past cold periods such as the Little Ice Age (LIA) (Koppes and Hallet, 2002; Hodder et al., 2007). However, grain-size versus thickness correlation suggests that the relationship between the intensity of flood events and the volume of transported material remained constant and was not affected by glacial cover (Fig. 3, Wilhelm et al., 2012b, 2013; Fouinat et al., 2017). Moreover, no glacial moraine is present in the watershed. Finally, the main transported sediment stream is oriented towards the south, thus limiting the effect of permafrost activity during Holocene cold periods.

5.3.2. Human activity

Lake sediment aDNA was used in this study to trace relationships between past landscape changes and past agro-pastoralism activities (mammal DNA). At this altitude, the presence of aDNA from domestic animals may be considered as a proxy for changes in grazing intensity (Etienne et al., 2013; Giguet-Covex et al., 2014; Wilhelm et al., 2016a). An increase of grazing pressure that affected both vegetal cover and soil erodibility by trampling may have made soils more vulnerable to erosion during heavy rainfalls, which led to an increasing erosion rate, and consequently, an increased sensitivity of the catchment-lake system to record flood events (Giguet-Covex et al., 2012). Mammal aDNA shows the presence of ovines and bovines in the Savine catchment only during the restricted period between 2.05 and 1.75 kyr cal BP, known as the Roman Period (Fig. 6E and F). The Roman Period with high pastoralism activity is synchronous in the Anterne lake record with the presence of both ovine and bovine herds (Giguet-Covex et al., 2014). Arnaud et al. (2016) recently noted that such an increase in human activity during the Roman Period appears to have been regional at the scale of the Northern French Alps. Indeed, the same pattern was recorded both at low (e.g., Lake Moras, Doyen et al. (2013), Lake Paladru, Simonneau et al. (2013)), intermediate (Lake La Thuile, Bajard et al., 2016) and high altitude (Lake Anterne, Giguet-Covex et al., 2011) resulting in a drastic rise in erosion fluxes for respective lakes. In Lake Anterne, Giguet-Covex et al. (2011) showed that this change of land use also resulted in the highest apparent flood frequency recorded for the Holocene (Fig. 6G) and in a distinct pattern in grain size versus flood layer thickness.

In Lake Savine, the flood frequency was relatively high during the first part of the period marked by high grazing pressure but less than during periods without grazing pressure, e.g., 5.3, 2.6, 1.7 or 0.3 kyr cal BP (Fig. 6B). Moreover, there was no change in grainsize versus event layer thickness patterns during this period (Fig. 3), as was observed at Lake Anterne because of grazing-induced changes in erosion processes (Giguet-Covex et al., 2011) or in Lake Allos in relation to human activities (Brisset et al., 2017). Therefore, it seems that the presence of ovine and bovine herds in the watershed had minor influences on the reconstructed flood chronicle.

However, the pastoralism phase corresponded to an increase in mean sedimentation rate (without flood layers) during this period. This suggests that herds and sediment sources transported during flood events were not at the same location of the watershed. The sediment source of flood events was in the southeastern part of the lake catchment with presence and probably reactivation of alluvial fans (Fig. 1), whereas the pastoralism activities were probably more restricted to the flat grassland part, i.e., close to the eastern lake shore and on the delta, as suggested by modern observations (Giguet-Covex and Walsh, pers. com.).

5.4. Palaeoflood activity

The comparison between ages of the recent flood deposits and dates of historical floods are in good agreement (Fig. 4). Moreover, significant changes in event layers related to erosion processes did not appear to be significantly linked to changes in geomorphological and/or human activities in the Savine watershed, which gives us confidence to interpret the Savine flood record from a paleoclimatic perspective.

5.4.1. Historical floods

Weather reanalysis of the last 8 floods recorded both in the Savine sediment sequence and in historical chronicles have been performed to better understand atmospheric circulation patterns (e.g., Rimbu et al., 2016). Two main groups of flood-prone synoptic configurations were identified from 500 hPa geopotential height

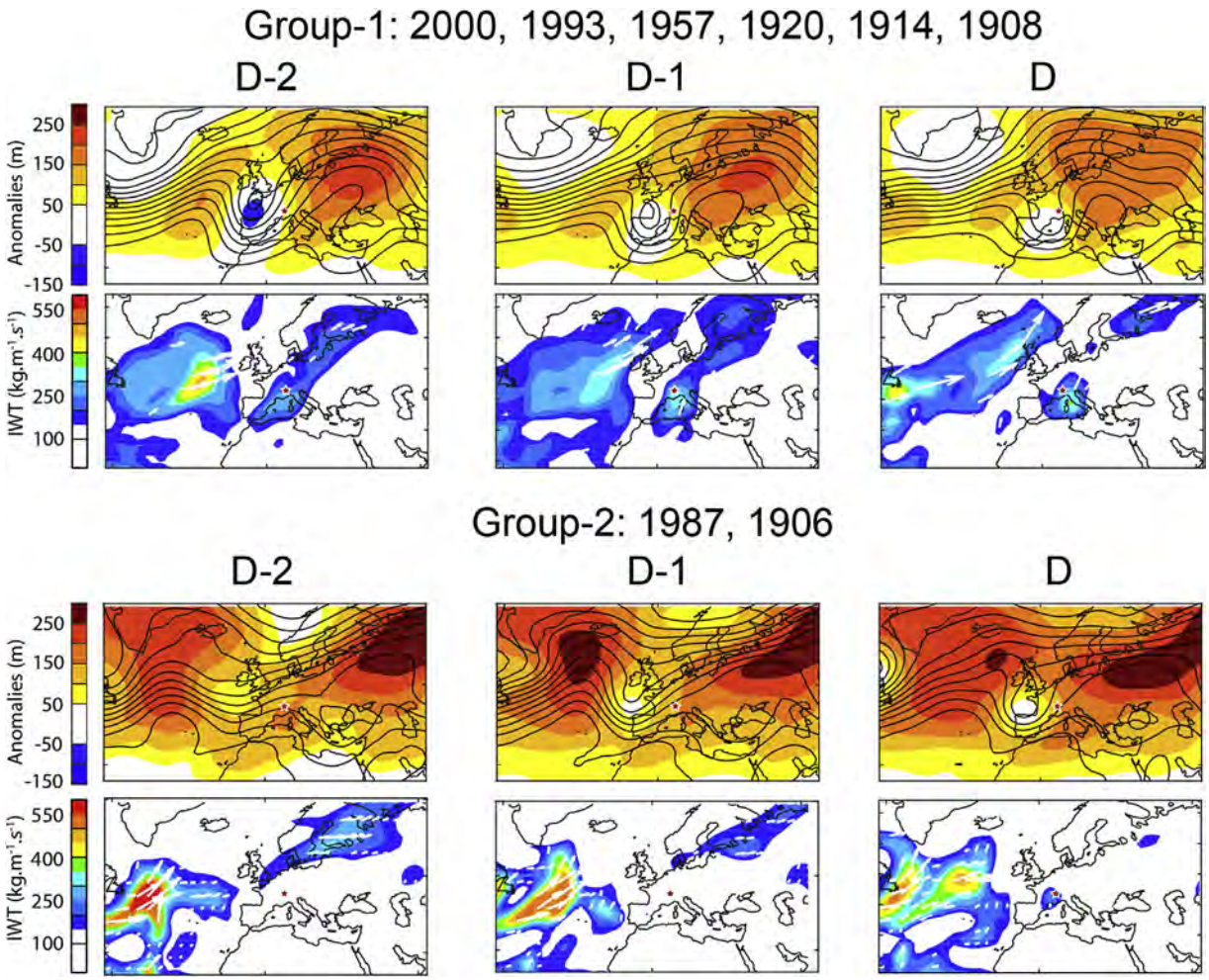

Fig. 7. Composite map of the 500 hPa geopotential heights (contour) and anomalies (shaded) and of IWT on the day of the historical flood (D) and the two days before (D-1 and D-2). Analysed events are those recorded in the sediment of Savine lake. The red star is the Savine lake location. (For interpretation of the references to colour in this figure legend, the reader is referred to the web version of this article.)

and IWT analysis (Fig. 7). The first group, named Group-1, corresponded to 6 of 8 flood events (15/10/2000, 24/09/1993, 12/06/1957, 24/09/1920, 23/07/1914 and 20/06/1908), and the second group, named Group-2, corresponded to 2 of 8 events (24/08/1987 and 03/07/1906). All these floods occurred between mid-June to mid-October. The 500 hPa geopotential height for Group-1 events showed a systematic low-pressure anomaly over the Bay of Biscay at D-2 that moved southeastward over the north Mediterranean area at D-1 and D. Such a pattern would trigger a cyclonic circulation around the low-pressure anomaly that would be expected to pick-up moisture from the Mediterranean Sea and favour rainfall on the Po Plain. This pattern resembles the weather pattern "WP6", identified from 1000 hPa geopotential height in Garavaglia et al. (2010), the so-called "East Return" events. The IWT for Group-1 events showed an increase of moisture in the northwestern Mediterranean area at D-2, followed by a moisture maxima and a marked advection northward into the Po Plain at D-1 and D. This atmospheric circulation pattern is typical of the late spring to autumn mesoscale events, called "East Return" events, whose circulation is associated with heavy rainfalls along the Italian border (Garavaglia et al., 2010; Gottardi et al., 2010; Lionello et al., 2012). The warm and humid air masses are vigorously uplifted by the Alpine orography, causing an abrupt cooling and intense precipitation typical of the Mediterranean climate. Two of the recorded Group-1 events (June 1957; October 2000) were regional catastrophic floods that affected many areas in the French and Italian Alps (Ratto et al., 2003; Arnaud-Fassetta and Fort, 2004). It is clear that such mesoscale precipitation events are the dominant mechanism that produces flood events recorded in the sediment sequence of Lake Savine. The geopotential height for Group-2 events shows a generalized high pressure anomaly over Europe, with two main centres located over north-eastern Eurasia and the northern Atlantic Ocean. This pattern triggers an anticyclonic circulation over the study area that hampers rainfall. It resembles the weather pattern "WP8" identified from 1000 hPa geopotential height in Garavaglia et al. (2010) that is associated with a lack of rain over Europe. The IWT for Group-2 events was null around the study site during D-2 and D-1, whereas low values of IWT were observed in a much more restricted continental area at D. The weak activity of the atmospheric circulation at the synoptic scale and the event layer occurrence during the summer season suggest that these two flood events resulted from localized phenomena such as thunderstorms.

5.4.2. *The Savine flood chronicle and climate forcing*

Because floods recorded during the last centuries were mainly triggered by mesoscale precipitation events, we assumed that the Savine palaeoflood record represented the variability of such

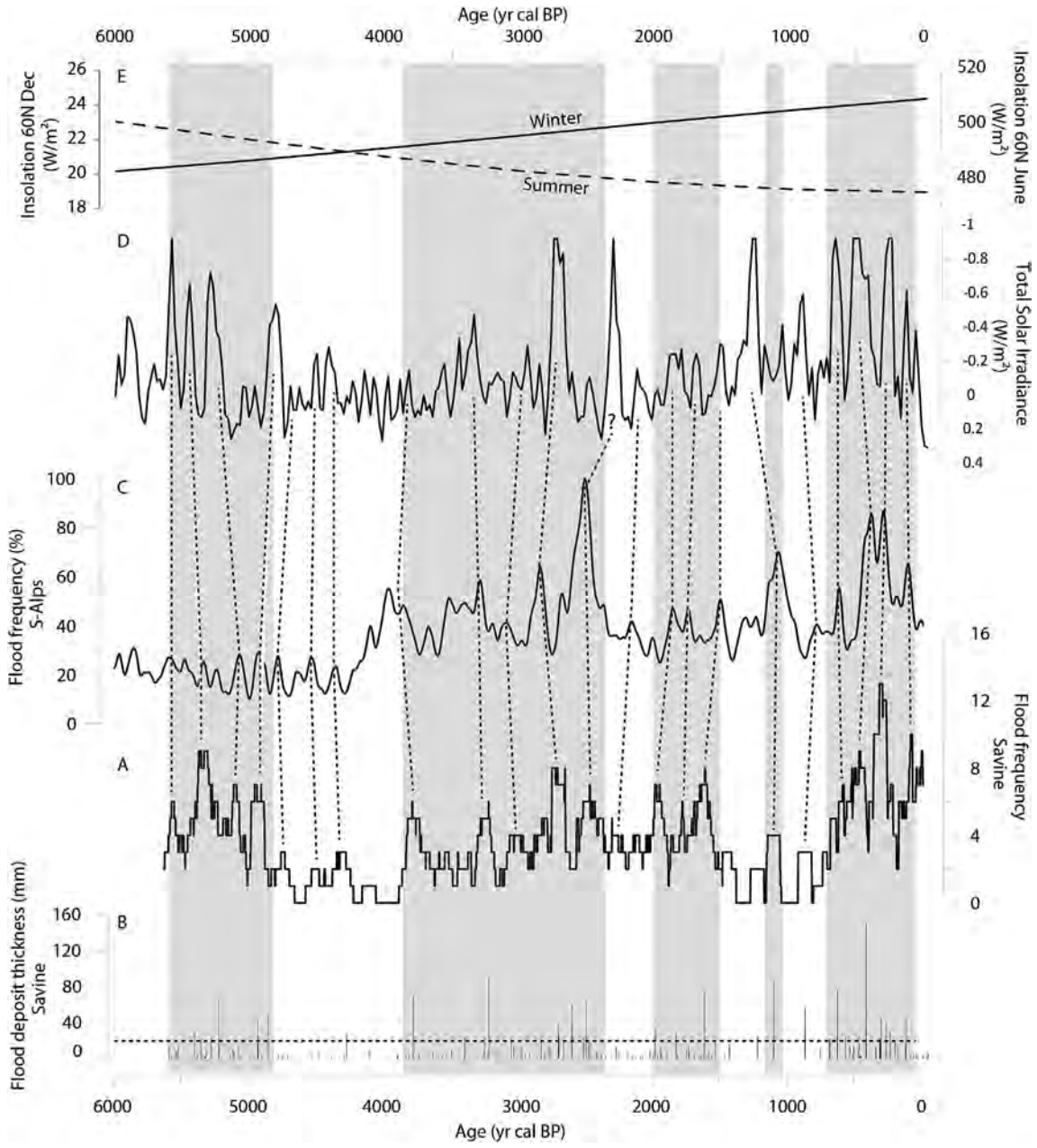

Fig. 8. Comparison of (A) reconstructed Savine flood frequency (101-yr running average) and (B) intensity (thickness of flood deposits) with (C) stacked S-Alps flood frequency (100-year low-pass filtered; Wirth et al., 2013), (D) Total Solar Irradiance (TSI) by Steinhilber et al. (2012) and (E) June and December insolation at 60°N (Berger and Loutre, 1991). Vertical grey areas mark high frequency and high intensity flood periods recorded for Lake Savine at a multi-centennial timescale. Dotted lines attempt to correlate, at a secular timescale, periods of high flood frequencies for Lake Savine with both high S-Alps flood frequencies and low solar activity periods; all these correlations are within the age model uncertainties.

events over the entire studied period (Fig. 8A and B). At a multi-centennial timescale, the Savine record showed five periods of high flood frequency between 5.6 and 4.85, 3.9–2.35, 2–1.5, 1.15–1.05 and 0.65–0.05 kyr cal BP. These increases in flood frequency were associated with the occurrence of the most intense floods (Fig. 8B). Only one intense flood occurred during a period of low flood frequency at approximately 900 yr cal BP. For the last millennium, higher flood frequency and intensity were thus recorded during the Little Ice Age (LIA, 1300 CE–1900) and lower flood frequency and intensity during the warmer Medieval Climate Anomaly (MCA, 800–1300 CE). Some events are possibly missed during cold years when the lake is covered by ice for longer than usual, such as during LIA. This suggests that there is a possibility that a flood event may occurs when the lake is still ice-bound and therefore not be recorded. However, we observed an increase of flood frequency during cold period, thus if the lake was ice covered during a longer period over a year, the interpretation does not change and could be consolidated. A similar pattern of flood frequency was observed in the European Alps (e.g., Glur et al., 2013; Swierczynski et al., 2013; Wirth et al., 2013; Wilhelm et al., 2013) and in the northwestern Mediterranean region (Moreno et al., 2008; Arnaud-Fassetta et al., 2010; Wilhelm et al., 2012a, 2016a; Benito et al., 2015). A similar pattern of flood intensity was also observed for Lake Allos, located 105 km south and strongly influenced by the Mediterranean climate (Wilhelm et al., 2012a).

Over the entire studied period, the Savine record seems similar

to the stacked flood-frequency records of the Southern Alps (Wirth et al., 2013), also strongly influenced by the Mediterranean climate (Fig. 8C). The Southern Alps record showed relatively low flood activity during the early Holocene followed by a sharp increase in flood frequency at 4.2 kyr cal BP that lasted for the entire Late Holocene. This main change at 4.2 kyr cal BP was also recorded in Lake Ledro (Vannière et al., 2013) and Lake Savine but was dated at 3.9 kyr cal BP at Lake Savine. This time lag between records may be linked to (i) the respective dating uncertainties (3.8–4.02 kyr cal BP for Lake Savine) or (ii) the more northern position of Lake Savine, which may explain a later impact of Mediterranean climate changes which propagate northward. Vannière et al. (2013) and Magny et al. (2013) attributed this transition to a nonlinear climate response to the orbital-driven gradual decrease in summer insolation at 60°N (Fig. 8E, Berger and Loutre, 1991). This would control the multi-millennial trend towards wetter conditions during the late Holocene (Mayewski et al., 2004). The Savine record also shows a generally higher level of flood frequency after 4.2 kyr cal BP, with peaks at 3.9–2.35, 2–1.5, 1.15–1.05 and 0.65–0.05 kyr cal BP. These peaks seem synchronous with the stacked S-Alps records (grey bands Fig. 8A, C) and mainly correspond to Holocene cold events (Bond et al., 2001; Mayewski et al., 2004; Wanner et al., 2011). These climate events are known to have produced a stronger meridional temperature gradient, and thus, a southward position of the westerlies with higher storm activity in the western Mediterranean region (Sabatier et al., 2012). The synchronism in flood frequency between Savine and the S-Alps records since 4.2 kyr cal BP seems still remarkable at the centennial timescale (dotted line in Fig. 8A, C). This supports the conclusion that both records were influenced by Mediterranean mesoscale precipitation events, as shown by historical events reanalysis. Before 4.2 kyr cal BP the Savine flood frequency presented a main increase between 5.6 and 4.85 kyr cal BP. This increase in flood frequency was not recorded in the Southern Alps but was visible in northern and central alpine records such as Lake Anterne (5.6–4.6 kyr cal BP, Giguet-Covex et al., 2011, Figs. 8B and 6G), Lake Bourget (centered at approximately 5.5 kyr cal BP, Arnaud et al., 2012), Ammersee (between 5.5 and 5 kyr cal BP, Czymzik et al., 2016) and in the N-Alps stack record (Wirth et al., 2013). Therefore, the flood frequency at Lake Savine seems to be in phase with the palaeoflood record of the Northern Alps before 4.2 kyr cal BP and with records of the Southern Alps after this period. Over the last millennium, floods in the Northern French Alps were mostly triggered by localized convective precipitation events during the summer (Wilhelm et al., 2013). Because floods at Lake Savine can also be triggered by thunderstorms, we propose that such processes could have been the dominant flood trigger prior to the 4.2 kyr cal BP climate transition.

The Savine flood frequency had 22 short term increases (dotted lines in Fig. 8), mostly associated with higher flood intensity. Each of these centennial increases seems to be synchronous with well-marked increases in Total Solar Irradiance (TSI, Fig. 8A, D; Steinhilber et al., 2012), which suggests an increasing flood frequency and intensity during periods of solar minima. Over the last 1.4 kyr cal BP, Wilhelm et al. (2012a) showed that major multi-centennial changes in flood frequency and intensity in the Southern Alps occurred during cooler periods such as the LIA and are associated with solar activity. Similarly, Wirth et al. (2013) suggested a strong solar influence on the Mediterranean precipitation regime because they observed a synchronism between low TSI values and high flood frequency. Similarly, in central Europe (southern Germany), Czymzik et al. (2016) found that flood frequency is higher when solar activity is reduced. Therefore, large changes in solar radiation (grand solar minima) indirectly affect climate by inducing atmospheric changes in the large European Atlantic sector (Martin-Puertas et al., 2012), which results in higher flood frequency and intensity in the Savine area. Several studies showed that periods of long-term reductions in solar radiation induced a North Atlantic storm track shift further to the south. Its maximum over the Mediterranean Sea, carried more humid air masses to central and southern Europe (e.g., Raible et al., 2007; Martin-Puertas et al., 2012). In this scenario, the part of the Alps influenced by the proximity of the Mediterranean climate likely experienced an increase in flood frequency and intensity because of increased moisture advection from the North Atlantic.

Finally, our results suggest that the occurrence and the intensity of extreme precipitation events that trigger mountain-river floods may be influenced by both lower temperatures on a millennial timescale and solar forcing through changes in atmospheric patterns on a centennial scale. Even if we cannot exclude future changes in TSI and its effect on flood occurrence, the current global temperature increases would lead to less extreme precipitation events in this area. However, higher temperatures would also lead to more efficient convective processes (Beniston et al., 2007; Giorgi et al., 2016), thereby producing heavy local rainfall events, and in turn, high intensity flood events, as they occurred prior to 4 kyr cal BP. Because this type of precipitation pattern accounts for a small part of historical events, we cannot exclude a future increase of this type of events resulting from unprecedented warming.

6. Conclusion

The high-resolution sedimentological and geochemical analyses of the sediment sequence from Lake Savine allowed the identification of 220 event layers for the last 6000 years. Twenty of the 220 event layers were differentiated by grain size parameters and geochemical features (low Mn contents) and most probably resulted from mass movements. These events were distributed in 5 clusters over this period and possibly related to earthquakes, considering their correlation to regional historic and paleo earthquakes. We found a strong relationship between deposit thickness and coarse fraction content (D90 max) for the other 200 event layers, which suggests that these event layers were produced by floods and that the thickness of deposits can be used as a high-resolution proxy for palaeoflood intensity. Local human activity was reconstructed through ancient DNA and revealed that ovines and bovines were present in the catchment area during a restricted period between 2.05 and 1.75 kyr cal BP. However, no change was observed in the grainsize versus deposit thickness pattern during this period, which suggests a minor influence of human activity on the reconstructed flood chronicle.

Weather reanalysis data for the time of historical floods recorded in the Savine sequence showed that the floods represented past variability of mainly mesoscale events, called “East Return” events (75%), and to a smaller extent, local summer convective events (i.e., thunderstorms). At a multi-centennial timescale, the Savine flood chronicle showed five periods of high flood frequency and intensity between 5.6 and 4.85, 3.9–2.35, 2–1.5, 1.15–1.05 and 0.65–0.05 kyr cal BP. These periods mainly correspond to Holocene cold events and agree well with previously reconstructed flood frequencies from the northern Alpine region between 6 and 4 kyr BP and from the southern Alpine region between 4 kyr cal BP and today. The paleohydrological transition at 4 kyr BP may have resulted from an abrupt change from Atlantic to Mediterranean climatic influences on the flood activity in the studied Alpine area and may correspond to the observed transition in the Mediterranean area during this period. At a centennial timescale, increases in flood frequency and intensity at Savine occurred during periods of solar minima. These long-term reductions in solar radiation probably indirectly affected the climate in a large European Atlantic sector through atmospheric changes, with a southward shift in the

North Atlantic storm tracks and a maximum over the Mediterranean Sea. During these periods, more humid air masses influenced by the proximity of the Mediterranean Sea were transported to the Alpine region and induced an increase in flood frequency and intensity.

Acknowledgements

This research was performed by the Hannibal Project funded by the DIPEE (Dispositifs de Partenariat en Ecologie et Environnement) Chambéry Grenoble of the CNRS INEE. We thank the municipality of Bramand for the coring authorization. The authors thank CLIMCOR Continent for coring facilities. ^{14}C analyses were acquired thanks to the CNRS-INSU ARTEMIS national radiocarbon AMS measurement programme at Laboratoire de Mesure 14C (LMC14) in the CEA Institute at Saclay (French Atomic Energy Commission). The authors thank the Laboratoire Souterrain de Modane (LSM) facilities for the gamma spectrometry measurements and Environnement, Dynamique et Territoires de Montagne for the X-ray fluorescence analyses. The authors wish to thank the editor Prof. Neil Roberts and the two anonymous reviewer who brought comments which greatly improved the original manuscript.

Appendix A. Supplementary data

Supplementary data related to this article can be found at http://dx.doi.org/10.1016/j.quascirev.2017.06.019.

References

Alric, B., Jenny, J.P., Berthon, V., Arnaud, F., Pignol, C., Reyss, J.L., Sabatier, P., Perga, M.E., 2013. Local forcings affect lake zooplankton vulnerability and response to climate warming. Ecology 94, 2767–2780.
Appleby, P.G., 1991. 241Am dating of lake sediments. Hydrobiologia 214, 35–42.
Arnaud, F., Lignier, V., Revel, M., Desmet, M., Beck, C., Pourchet, M., Charlet, F., Trentesaux, A., Tribovillard, N., 2002. Flood and earthquake disturbance of 210Pb geochronology (Lake Anterne, NW Alps). Terra Nova 14, 225–232.
Arnaud, F., Poulenard, J., Giguet-Covex, C., Wilhelm, B., Révillon, S., Jenny, J.P., Enters, D., Bajard, M., Fouinat, L., Doyen, E., Simonneau, A., Chapron, E., Vannière, B., Sabatier, P., 2016. Erosion under climate and human pressures : an alpine lake sediment perspective. Quat. Sci. Rev. 152, 1–18.
Arnaud-Fassetta, G., Fort, M., 2004. Respective parts of hydroclimatic and anthropic factors in the recent eveolution (1956–2000) of the active channel of the Upper Guil, Queyras, Southern French Alps. Méditerranée 102, 143–156.
Arnaud-Fassetta, G., Carcaud, N., Castanet, C., Salvador, P.G., 2010. Fluviatile palaeoenvironments in archaeological context: geographical position, methodological approach and global change hydrological risk issues. Quatern. Int. 216, 93–117.
Bajard, M., Sabatier, P., David, F., Develle, A.L., Reyss, J.L., Fanget, B., Malet, E., Arnaud, D., Augustin, L., Crouzet, C., Poulenard, J., Arnaud, F., 2016. Erosion record in Lake La Thuile sediments evidences montane landscape dynamics through the Holocene. Holocene 26 (3), 350–364.
Beck, C., 2009. Late Quaternary lacustrine paleo-seismic archives in north-western Alps: examples of earthquake-origin assessment of sedimentary disturbances. Earth Sci. Rev. 96, 327–344.
Beniston, M., Stephenson, D.B., 2004. Extreme climatic events and their evolution under changing climatic conditions. Glob. Planet. Change 44, 1–9.
Beniston, M., Stephenson, D.B., Christensen, O.B., Christopher, A., Ferro, T., Frei, C., Goyette, S., Halsnaes, K., Holt, T., Jylhä, K., Koffi, B., Palutikof, J., Schöll, R., Semmler, T., Woth, K., T, 2007. Future extreme events in European climate: an exploration of regional climate model projections. Clim. Change 81, 71–95.
Berger, A., Loutre, M.F., 1991. Insolation values for the climate of the last 10 million years. Quat. Sci. Rev. 10, 297–317.
Benito, G., Macklin, M.G., Zielhofer, C., Jones, A., Machado, M.J., 2015. Holocene flooding and climate change in the Mediterranean. Catena 130, 13–33.
Blaauw, M., 2010. Methods and code for 'classical' age-modelling of radiocarbon sequences. Quat. Geochronol. 5 (5), 512–518.
Bøe, A.-G., Dahl, S.O., Lie, Ø., Nesje, A., 2006. Holocene river floods in the upper Glomma catchment, southern Norway: a high-resolution multiproxy record from lacustrine sediments. Holocene 16, 445–455.
Bond, G., Kromer, B., Beer, J., Muscheler, R., Evans, M.N., Showers, W., Hoffmann, S., Lotti-Bond, R., Hajdas, I., Bonani, G., 2001. Persistent solar influence on north atlantic climate during the Holocene. Science 294, 2130–2136.
Boschi, E., Guidoboni, E., Ferrari, G., Mariotti, D., Valensise, G., Gasperini, P. (Eds.), 2000. Catalogue of Strong Italian Earthquakes from 461 B.C. To 1997. Introductory Texts and CD-ROM, vol. 43. Annali di Geofisica, p. 4.
Boyer, F., Mercier, C., Bonin, A., Le Bras, Y., Taberlet, P., Coissac, E., 2016. obitools: a unix-inspired software package for DNA metabarcoding. Mol. Ecol. Resour. 16, 176–182.
Brisset, E., Guitter, F., Miramont, C., Troussier, T., Sabatier, P., Poher, Y., Cartier, R., Arnaud, F., Malet, E., Anthony, E., 2017. Floods aggravated by Humans : lessons from the past. Geology. http://dx.doi.org/10.1130/G38498.1.
Campbell, C., 1998. Late Holocene lake sedimentology and climate change in southern Alberta, Canada. Quat. Res. 49, 96–101.
Calvert, S.E., Pedersen, T.F., 1993. Geochemistry of recent oxic and anoxic marine sediments: implications for the geological record. Mar. Geol. 113 (1), 67–88.
CEA, 2007. Reducing the Social and Economic Impact of Climate Change and Natural Catastrophes: Insurance Solutions and Public Private Partnerships. Insurers of Europe, Brussels.
Chapron, E., Beck, C., Pourchet, M., Deconinck, J.-F., 1999. 1822 AD earthquake-triggered homogenite in Lake Le Bourget (NW Alps). Terra Nova 11, 86–92.
Chapron, E., Simonneau, A., Ledoux, G., Arnaud, F., Lajeunesse, P., Albéric, P., 2016. French alpine foreland Holocene paleoseismicity revealed by coeval mass wasting deposits in glacial lakes (Chapter 34). In: Lamarche, G., et al. (Eds.), Submarine Mass Movements and Their Consequences, Advances in Natural and Technological Hazards Research, vol. 41. Springer International Publishing Switzerland 2016, pp. 341–349.
Compo, G.P., Whitaker, J.S., Sardeshmukh, P.D., Matsui, N., Allan, R.J., Yin, X., Gleason, B.E., Vose, R.S., Rutledge, G., Bessemoulin, P., Bronnimann, S., Brunet, M., Crouthamel, R.I., Grant, A.N., Groisman, P.Y., Jones, P.D., Kruk, M., Kruger, A.C., Marshall, G.J., Maugeri, M., Mok, H.Y., Nordli, O., Ross, T.F., Trigo, R.M., Wang, X.L., Woodruff, S.D., Worley, S.J., 2011. The twentieth century reanalysis Project. Q. J. R. Meteorol. Soc. 137, 1–28.
Corella, J.P., Benito, G., Rodriguez-Lloveras, X., Brauer, A., Valero-Garcès, B., 2014. Annually-resolved lake record of extreme hydro-meteorological events since AD 1347 in NE Iberian Peninsula. Quat. Sci. Rev. 93, 77–90.
Czymzik, M., Muscheler, R., Brauer, A., 2016. Solar modulation of flood frequency in central Europe during spring and summer on interannual to multi-centennial timescales. Clim. Past 12, 799–805.
Doyen, E., Vanniere, B., Berger, J.-F., Arnaud, F., Tachikawa, K., Bard, E., 2013. Land-use changes and environmental dynamics in the upper Rhone valley since Neolithic times inferred from sediments in Lac Moras. Holocene 23, 961–973. http://dx.doi.org/10.1177/0959683612475142.
Durant, Y., Laternser, M., Giraud, G., Etchevers, P., Lesaffre, B., Merindol, L., 2009. Reanalysis of 44 Yr of climate in the French Alps (1958–2002): methodology, model validation, climatology, and trends for air temperature and precipitation. J. Appl. Meteorol. Climatol. 48, 429–449.
Elbaz-Poulichet, F., Sabatier, P., Dezileau, L., Freydier, R., 2014. Sedimentary record of V, U, Mo and Mn in the Pierre-Blanche lagoon (Southern France) - evidence for a major anoxia event during the Roman period. Holocene 24 (10), 1384–1392.
Etienne, D., Wilhelm, B., Sabatier, P., Reyss, J.-L., Arnaud, F., 2013. Influence of sample location and livestock numbers on Sporormiella concentrations and accumulation rates in surface sediments of Lake Allos, French Alps. J. Paleolimnol. 49, 117–127.
Ficetola, G.F., Taberlet, P., Coissac, E., 2016. How to limit false positives in environmental DNA and metabarcoding? Mol. Ecol. Resour. 16, 604–607.
Ficetola, G.F., Pansu, J., Bonin, A., Coissac, E., Giguet-Covex, C., De Barba, M., Gielly, L., Martins Lopes, C., Boyer, F., Pompanon, F., Rayé, J., Taberlet, P., 2015. Replication levels, false presences, and the estimation of presence/absence from eDNA metabarcoding data. Mol. Ecol. Resour. 15, 543–556.
Fouinat, L., Sabatier, P., Poulenard, P., Etienne, D., Crouzet, C., Develle, A.L., Doyen, E., Malet, E., Reyss, J.L., Bonnet, R., Arnaud, F., 2017. 1700 years of interaction between glacial activity and flood frequency in proglacial Lake Muzelle (western French Alps). Quat. Res. 87 (03), 407–422.
Garavaglia, F., Gailhard, J., Paquet, E., Lang, M., Garcon, R., Bernardara, P., 2010. Introducing a rainfall compound distribution model based on weather patterns sub-sampling. Hydrol. Earth Syst. Sci. 14, 951–964.
Gaume, E., Bain, V., Bernardara, P., Newinger, O., Barbuc, M., Bateman, A., Blaškovicová, L., Blöschl, G., Borga, M., Dumitrescu, A., Daliakopoulos, I., Garcia, J., Irimescu, A., Kohnova, S., Koutroulis, A., Marchi, L., Matreata, S., Medina, V., Preciso, E., Sempere-Torres, D., Stancalie, G., Szolgay, J., Tsanis, I., Velasco, D., Viglione, A., 2009. A compilation of data on European flash floods. J. Hydrology 367, 70–78.
Giguet-Covex, C., Arnaud, F., Poulenard, J., Disnar, J.-R., Delhon, C., Francus, P., David, F., Enters, D., Rey, P.-J., Delannoy, J.-J., 2011. Changes in erosion patterns during the Holocene in a currently treeless subalpine catchment inferred from lake sediment geochemistry (Lake Anterne, 2063 m a.s.l., NW French Alps): the role of climate and human activities. Holocene 21, 651–665. http://dx.doi.org/10.1177/0959683610391320.
Giguet-Covex, C., Arnaud, F., Enters, D., Poulenard, J., Millet, L., Francus, P., David, F., Rey, P.-J., Wilhelm, B., Delannoy, J.-J., 2012. Frequency and intensity of high-altitude floods over the last 3.5ka in northwestern French Alps (Lake Anterne). Quat. Res. 77, 12–22. http://dx.doi.org/10.1016/j.yqres.2011.11.003.
Giguet-Covex, C., Pansu, J., Arnaud, F., Rey, P.-J., Griggo, C., Gielly, L., Domaizon, I., Coissac, E., David, F., Choler, P., 2014. Long livestock farming history and human landscape shaping revealed by lake sediment DNA. Nat. Commun. 5 http://dx.doi.org/10.1038/ncomms4211.
Gilbert, R., Crookshanks, S., Hodder, K.R., Spagnol, J., Stull, R.B., 2006. The record of an extreme flood in the sediments of montane Lillooet Lake, British Columbia: implications for paleoenvironmental assessment. J. Paleolimnol. 35, 737–745.

Gilli, A., Anselmetti, F.S., Glur, L., Wirth, S.B., 2013. Lake sediments as archives of recurrence rates and intensities of past flood events. Adv. Global Change Res. In: Schneuwly-Bollschweiler, M., Stoffel, M., Rudolf-Miklau, F. (Eds.), Dating Torrential Processes on Fans and Cones – Methods and Their Application for Hazard and Risk Assessment, vol. 47, pp. 225–242.

Giorgi, F., Torma, C., Coppola, E., Ban, N., Schär, C., Somot, S., 2016. Enhanced summer convective rainfall at Alpine high elevations in response to climate warming. Nat. Geosci. http://dx.doi.org/10.1038/NGEO2761.

Glur, L., Wirth, S.B., Buntgen, U., Gilli, A., Haug, G.H., Schär, C., Beer, J., Anselmetti, F.S., 2013. Frequent floods in the European Alps coincide with cooler periods of the past 2500 years. Sci. Rep. 3, 2770. http://dx.doi.org/10.1038/srep02770.

Golberg, E., 1963. Geochronology with 210Pb. Radioactive Dating. International Atomic Energy Agency, Vienna, pp. 121–131.

Gottardi, F., Obled, C., Gailhard, J., Paquet, E., 2010. Statistical reanalysis of precipitation fields based on ground network data and weather patterns: application over French mountains. J. Hydrol. 432/433, 154–167.

Guédron, S., Amouroux, D., Sabatier, P., Desplanque, C., Develle, A.L., Barre, J., Feng, C., Guiter, F., Arnaud, F., Reyss, J.L., Charlet, L., 2016. A 150-year record of industrial and urban development in French Alps combining Hg accumulation rates and isotope composition in sediment archives from Lake Luitel. Chem. Geol. 431, 10–19.

Heiri, O., Lotter, A.F., Lemcke, G., 2001. Loss on ignition as a method for estimating organic and carbonate content in sediments: Reproducibility and comparability of results. J. Paleolimnol. 25 (1), 101–110.

Hodder, K.R., Gilbert, R., Desloges, J.R., 2007. Glaciolacustrine varved sediment as an alpine hydroclimatic proxy. J. Paleolimnol. 38, 365–394.

IPCC, 2013. In: Stocker, T.F., Qin, D., Plattner, G.-K., Tignor, M., Allen, S.K., Boschung, J., Nauels, A., Xia, Y., Bex, V., Midgley, P.M. (Eds.), The Physical Science Basis, Contribution of Working Group I to the Fifth Assessment Report of the Intergovernmental Panel on Climate Change. Cambridge University Press, Cambridge, United Kingdom and New York, NY, USA.

Jenny, J.P., Arnaud, F., Dorioz, J.M., Giguet Covex, C., Frossard, V., Sabatier, P., Millet, L., Reyss, J.L., Tachikawa, K., Bard, E., Pignol, C., Perga, M.E., 2013. A spatiotemporal sediment investigation highlights the dynamics of hypolimnetic hypoxia in large perialpine Lake Bourget over the last 150 years. Limnol. Oceanogr. 58, 1395–1408.

Jenny, J.P., Wilhelm, B., Arnaud, F., Sabatier, P., Giguet Covex, C., Mélo, A., Fanget, B., Malet, E., Ployon, E., Perga, M.E., 2014. A 4D sedimentological approach to reconstructing the flood frequency and intensity of the Rhône River (Lake Bourget, NW European Alps). J. Paleolimnol. 51, 469–483.

Koppes, M.N., Hallet, B., 2002. Influence of rapid glacial retreat on the rate of erosion by tidewater glaciers. Geology 30, 47–50.

Lambert, J., Levret-Albaret, A., 1996, 78. In: Catalogues d'Épicentres, Paramètres et Références, Ouest-Editions (Eds.), Mille ans de Séismes en France. Presses Académiques, Nantes.

Lapointe, F., Francus, P., Lamoureux, S.F., Saıd, M., Cuven, S., 2012. 1750 years of large rainfall events inferred from particle size at East Lake, Cape Bounty, Melville Island, Canada. J. Paleolimnol. 48, 159–173.

Lionello, P., Abrantes, F., Congedi, L., Dulac, F., Gacic, M., Gomis, D., Goodess, C., Hoff, H., Kutiel, H., Luterbacher, J., Planton, S., Reale, M., Schröder, K., Struglia, M.V., Toreti, A., Tsimplis, M., Ulbrich, U., Xoplaki, E., 2012. Introduction: mediterranean climate: background information. In: Lionello, P. (Ed.), The Climate of the Mediterranean Region, from the Past to the Future. Elsevier (Netherlands), Amsterdam. XXXV–lXXX, ISBN:9780124160422.

Lahoz-Monfort, J.J., Guillera-Arroita, G., Tingley, R., 2016. Statistical approaches to account for false positive errors in environmental DNA samples. Mol. Ecol. Resour. 16, 673–685.

Magny, M., Combourieu Nebout, N., de Beaulieu, J.L., Bout-Roumazeilles, V., Colombaroli, D., Desprat, S., Francke, A., Joannin, S., Peyron, O., Revel, M., Sadori, L., Siani, G., Sicre, M.A., Samartin, S., Simonneau, A., Tinner, W., Vannière, B., Wagner, B., Zanchetta, G., Anselmetti, F., Brugiapaglia, E., Chapron, E., Debret, M., Desmet, M., Didier, J., Essallami, L., Galop, D., Gilli, A., Haas, J.N., Kallel, N., Millet, L., Stock, A., Turon, J.L., Wirth, S., 2013. North–south palaeohydrological contrasts in the central Mediterranean during the Holocene: tentative synthesis and working hypotheses. Clim. Past. 9, 1901–1967.

Martin-Puertas, C., Matthes, K., Brauer, A., Muscheler, R., Hansen, F., Petrick, C., Aldahan, A., Possnert, G., van Geel, B., 2012. Regional atmospheric circulation shifts induced by a grand solar minimum. Nat. Geosci. 5, 397–401.

Mayewski, P.A., Rohling, E.E., Stager, J.C., Karlen, W., Maasch, K.A., Meeker, L.D., Meyerson, E.A., Gasse, F., van Kreveld, S., Holmgren, K., Lee-Thorp, J., Rosqvist, G., Rack, F., Staubwasser, M., Schneider, R.R., Steig, E.J., 2004. Holocene climate variability. Quat. Res. 62, 243–255.

Molinaroli, E., Guerzoni, S., De Falco, G., Sarretta, A., Cucco, A., Como, S., 2009. Relationships between hydrodynamic parameters and grain size in two contrasting transitional environments: the lagoons of Venice and Cabras, Italy. Sediment. Geol. 219, 196–207.

Moreno, A., Valero-Garces, B.L., Gonzalez-Samperiz, P., Rico, M., 2008. Flood response to rainfall variability during the last 2000 years inferred from the Taravilla Lake record (Central Iberian Range, Spain). J. Palaeolimnol. 40, 943–961.

Mulder, T., Cochonat, P., 1996. Classification of offshore mass movements. J. Sediment. Res. 66, 43–57.

Mulder, T., Migeon, S., Savoye, B., Faugères, J.C., 2001. Inversely graded turbidite sequences in the deep Mediterranean: a record of deposits from flood-generated turbidity currents? Geo-Mar. Lett. 21, 86–93.

Noren, A.J., Bierman, P.R., Steig, E.J., Lini, A., Southon, J., 2002. Millennial-scale storminess variability in the northeastern United States during the Holocene epoch. Nature 419, 821–824.

Pansu, J., Giguet-Covex, C., Ficetola, G.F., Gielly, L., Boyer, F., Zinger, L., Arnaud, F., Poulenard, J., Taberlet, P., Choler, P., 2015. Reconstructing long-term human impacts on plant communities: an ecological approach based on lake sediment DNA. Mol. Ecol. 24, 1485–1498.

Parris, A.S., Bierman, P.R., Noren, A.J., Prins, M.A., Lini, A., 2010. Holocene paleostorms identified by particle size signatures in lake sediments from the northeastern United States. J. Paleolimnol. 43 (1), 29–49.

Passega, R., 1964. Grain-size representation by CM patterns as a geological tool. J. Sediment. Petrol. 34 (4), 830–847.

Pedersen, T.F., Price, N.B., 1982. The geochemistry of manganese carbonate in Panama Basin sediments. Geochimica Cosmochimica Acta 46 (1), 59–68.

Petersen, J., Wilhelm, B., Revel, M., Rolland, Y., Crouzet, C., Arnaud, F., Magand, O., Chaumillon, E., 2014. Sediment archive of Lake Vens (SW European Alps, France) as a record of large magnitude earthquakes. J. Paleolimnol 51, 343–355.

R Development Core Team, 2011. R: a Language and Environment for Statistical Computing. R Foundation for Statistical Computing, Vienna. Available at: http://www.R-project.org/.

Raible, C.C., Yoshimori, M., Stocker, T.F., Casty, C., 2007. Extreme midlatitude cyclones and their implications for precipitation and wind speed extremes in simulations of the Maunder Minimum versus present day conditions. Clim. Dynam. 28, 409–423.

Ratto, S., Bonetto, F., Comoglio, C., 2003. The October 2000 flooding in Valle d'Aosta (Italy): event description and land planning measures for the risk mitigation. Int. J. River Basin Manag. 1 (2), 105–116.

Ratzov, G., Cattaneo, A., Babonneau, N., Déverchère, J., Yelles, K., Bracene, R., Courboulex, F., 2015. Holocene turbidites record earthquake supercycles at a slow-rate plate boundary. Geology 43 (4), 331–334.

Reimer, P.J., Bard, E., Bayliss, A., Beck, J.W., Blackwell, P.G., Bronk Ramsey, C., Buck, C.E., Cheng, H., Edwards, R.L., Friedrich, M., others, 2013. IntCal13 and Marine13 Radiocarbon Age Calibration Curves 0-50,000 Years Cal BP.

Reyss, J.L., Schimdt, S., Legeleux, F., Bonte, P., 1995. Large low background well type detectors for measurements of environmental radioactivity. Nucl. Instrum. Methods 357, 391–397.

Richter, T.O., Van der Gaast, S.J., Koster, B., Vaars, A.J., Gieles, R., De Stigter, H.C., De Haas, H., VanWeering, T.C.E., 2006. The Avaatech XRF Core Scanner: technical description and applications to NE Atlantic sediments. In: Rothwell, R.G. (Ed.), NewTechniques in Sediment Core Analysis. : Special Publications. Geological Society, London, pp. 39–50.

Rimbu, N., Czymzik, M., Ionita, M., Lohmann, G., Brauer, A., 2016. Atmospheric circulation patterns associated with the variability of River Ammer floods: evidence from observed and proxy data. Clim. Past. 12, 377–385.

Sabatier, P., Dezileau, L., Colin, C.M., Briqueu, L., Martinez, P., Siani, G., Bouchette, F., Raynal, O., Von Grafenstein, U., 2012. 7000 years of paleostorm activity in the NW Mediterranean Sea in response to Holocene climate events. Quarternary Res. 77, 1–11.

Sabatier, P., Poulenard, J., Fanget, B., Reyss, J.L., Develle, A.L., Wilhelm, B., Ployon, E., Pignol, C., Naffrechoux, E., Dorioz, J.M., Montuelle, B., Arnaud, F., 2014. Secular interplays between pesticides and erosion in vineyards. PNAS 111 (44), 15647–15652.

Schiefer, E., Gilbert, R., Hassan, M.A., 2011. A lake sediment-based proxy of floods in the Rocky Mountain Front Ranges, Canada. J. Paleolimnol. 45, 137–149.

Scotti, O., Baumont, D., Quenet, G., Levret, A., 2004. The French macroseismic database SISFRANCE: objectives, results and perspectives. Ann. Geophys. 47 (2), 571–581.

Simonneau, A., Doyen, E., Chapron, E., Millet, L., Vannière, B., Di Giovanni, C., Bossard, N., Tachikawa, K., Bard, E., Albéric, P., Desmet, M., Roux, G., Lajeunesse, P., Berger, J.F., Arnaud, F., 2013. Holocene land-use evolution and associated soil erosion in the French Prealps inferred from Lake Paladru sediments and archaeological evidences. J. Archaeol. Sci. 40, 1636–1645. http://dx.doi.org/10.1016/j.jas.2012.12.002.

Steinhilber, F., Abreu, J.A., Beer, J., Brunner, I., Christ l, M., Fischer, H., Heikkilä, U., Kubik, P.W., Mann, M., McCracken, K., Miller, H., Miyahara, H., Oerter, H., Wilhelms, F., 2012. 9,400 years of cosmic radiation and solar activity from ice cores and tree rings. PNAS 109, 5967.

Sturm, M., Matter, A., 1978. Turbidites and varves in Lake Brienz (Switzerland): deposition of clastic detritus by density currents. Special Publ. Int. Assoc. Sedimentologists 2, 147–168.

Swierczynski, T., Lauterbach, S., Dulski, P., Delgado, J., Merz, B., Brauer, A., 2013. Mid- to late Holocene flood frequency changes in the northeastern Alps as recorded in varved sediments of Lake Mondsee (Upper Austria). Quat. Sci. Rev. 80, 78–90.

Taberlet, P., Prud'homme, S.M., Campione, E., Roy, J., Miquel, C., Shehzad, W., Gielly, L., Rioux, D., Choler, P., Clement, J.C., Melodelima, C., Pompanon, F., Coissac, E., 2012. Soil sampling and isolation of extracellular DNA from large amount of starting material suitable for metabarcoding studies. Mol. Ecol. 21, 1816–1820.

Vannière, B., Magny, M., Joannin, S., Simonneau, A., Wirth, S.B., Hamann, Y., Chapron, E., Gilli, A., Desmet, M., Anselmetti, F.S., 2013. Orbital changes, variation in solar activity and increased anthropogenic activities: controls on the Holocene flood frequency in the Lake Ledro area, Northern Italy. Clim. Past. 9, 1193–1209.

Wanner, H., Solomina, O., Grosjean, M., Ritz, S.P., Jetel, M., 2011. Structure and origin

of Holocene cold events. Quat. Sci. Rev. 30, 3109–3123.
Westra, S., Alexander, L.V., Zwiers, F.W., 2013. Global increasing trends in annual maximum daily precipitation. J. Clim. 26, 3904–3918.
Whitaker, J.S., Hamill, T.M., 2002. Ensemble data assimilation without perturbed observations. Mon. Weather Rev. 130, 1913–1924.
Wilhelm, B., Arnaud, F., Sabatier, P., Crouzet, C., Brisset, E., Chaumillon, E., Disnar, J.R., Guiter, F., Malet, E., Reyss, J.L., Tachikawa, K., Bard, E., Delannoy, J.J., 2012a. 1.4 kyrs of flash flood events in the Southern European Alps : implications for extreme precipitation patterns and forcing over the north western Mediterranean area. Quat. Res. 78, 1–12.
Wilhelm, B., Arnaud, F., Enters, D., Allignol, F., Legaz, A., Magand, O., Revillon, S., Giguet-Covex, C., Malet, E., 2012b. Does global warming favour the occurrence of extreme floods in European Alps? First evidences from a NW Alps proglacial lake sediment record. Clim. Change. http://dx.doi.org/10.1007/s10584-011-0376-2.
Wilhelm, B., Vogel, H., Crouzet, C., Etienne, D., Anselmetti, F.S., 2016a. Frequency and intensity of palaeofloods at the interface of Atlantic and Mediterranean climate domains. Clim. Past. 12, 299–316.
Wilhelm, B., Nomade, J., Crouzet, C., Litty, C., Sabatier, P., Belle, S., Rolland, Y., Revel, M., Courboulex, F., Arnaud, F., Anselmetti, F.S., 2016b. Quantified sensitivity of lake sediments to record historic earthquakes : implications for paleoseismology. J. Geophys. Res. 121 (1), 2–16.
Wilhelm, B., Arnaud, F., Sabatier, P., Magand, O., Chapron, E., Courp, T., Tachikawa, K., Fanget, B., Malet, E., Pignol, C., Bard, E., Delannoy, J.J., 2013. Palaeoflood activity and climate change over the last 1400 years recorded by lake sediments in the north-west European Alps. J. Quat. Sci. 28, 189–199.
Wilhelm, B., Sabatier, P., Arnaud, F., 2015. Is a regional flood signal reproducible from lake sediments? Sedimentology 62, 1103–1117.
Wirth, S.B., Glur, L., Gilli, A., Anselmetti, F.S., 2013. Holocene flood frequency across the Central Alps – solar forcing and evidence for variations in North Atlantic atmospheric circulation. Quat. Sci. Rev. 80, 112–128.